Neurobiology of Disease

Positron Emission Tomography (PET) Neuroimaging of the *Pink1-/-* Rat Parkinson Disease Model with the Norepinephrine Transporter (NET) Ligand [^{18}F]NS12137

Alexander K. Converse,[1] Maryann N. Krasko,[2,3] Denis Michael Rudisch,[2,3,4] Maxim S. Slesarev,[1] John C. Szot,[2] Catherine L. Gallagher,[5] and Michelle R. Ciucci[2,3,4,6]

[1]Waisman Center, University of Wisconsin-Madison Madison, Wisconsin 53705, [2]Department of Communication Science and Disorders, University of Wisconsin-Madison Madison, Wisconsin 53706, [3]Department of Surgery-Division of Otolaryngology, University of Wisconsin-Madison Madison, Wisconsin 53792, [4]UW Institute for Clinical and Translational Research, University of Wisconsin-Madison Madison, Wisconsin 53705, [5]Department of Neurology, University of Wisconsin-Madison; William S. Middleton VA Hospital Madison, Wisconsin 53705, and [6]Neuroscience Training Program, University of Wisconsin-Madison Madison, Wisconsin 53705

Evidence suggests that the neurotransmitter norepinephrine may play an important role in Parkinson disease (PD). The norepinephrine transporter (NET) regulates noradrenergic signaling and can serve as an index of noradrenergic innervation in neuroimaging studies. The *Pink1-/-* rat model, which exhibits many signs similar to PD, notably in the nonmotor domain, exhibits abnormal noradrenergic markers. Here, we sought to (1) implement reference region pharmacokinetic modeling of positron emission tomography (PET) imaging with the novel NET ligand [^{18}F]NS12137, (2) validate the resulting indices of NET concentration, and (3) characterize NET in the *Pink1-/-* model. Long–Evans *Pink1-/-* male rats were imaged by PET with [^{18}F]NS12137 at 9 and 11 months and compared with wild-type (WT) controls. An additional group of WT rats of both sexes were imaged with [^{18}F]NS12137 PET after pretreatment with the specific and selective NET ligand nisoxetine. Binding in locus coeruleus (LC), thalamus (Thal), and prelimbic area (PrL), regions rich in NET, was analyzed by a two-tissue compartment reversible binding model using a cerebellar reference region. [^{18}F]NS12137 binding exhibited moderate test–retest reproducibility in LC, Thal, and PrL. Nisoxetine blockade yielded substantial reductions of [^{18}F]NS12137 binding in LC. Compared with WT controls, *Pink1-/-* rats exhibited reduced binding in Thal and PrL. Pharmacokinetic analysis of [^{18}F]NS12137 PET provides a reproducible and specific measure of NET binding and indicates reduced NET in PD-related brain regions in *Pink1-/-* rats. Noninvasive in vivo [^{18}F]NS12137 PET imaging is therefore a promising method for the study of potential therapies in the *Pink1-/-* rat.

Key words: [18F]NS12137; noradrenaline; norepinephrine transporter; Parkinson's disease; Pink1-/- rat; prelimbic area

Significance Statement

Many signs of Parkinson disease (PD), particularly nonmotor ones, are associated with dysfunction of the noradrenergic system. However, pharmacological and behavioral therapies that target norepinephrine are not well developed for PD. It is important therefore to apply new tools for evaluating the noradrenergic effects of interventions in animal models of PD. In this work, we validated positron emission tomography (PET) neuroimaging in rats with the novel norepinephrine transporter (NET) radiotracer [^{18}F]NS12137. We also found reduced NET expression in important brain regions (thalamus and prelimbic area) in the *Pink1-/-* rat model of PD. [^{18}F]NS12137 PET is therefore a promising tool for trials of interventions in the *Pink1-/-* rat, and such work may lead to improved treatments for PD.

Received Feb. 4, 2025; revised March 26, 2025; accepted May 23, 2025.

Author contributions: A.K.C. and M.R.C. designed research; A.K.C., M.S.S., and J.C.S. performed research; A.K.C. analyzed data; A.K.C., M.N.K., D.M.R., and C.L.G. wrote the paper.

This work was supported by NIH NIDCD R01DC018584 (M.R.C) and F31DC022161 (M.N.K) and NIH NICHD P50HD105353. We are grateful to Dr. Jonathan Engle and the UW-Madison Medical Physics cyclotron staff, Dr. Bradley Christian and the UW-Madison Waisman Center Brain Imaging Core staff, and the UW-Madison laboratory animal veterinary staff.

The authors declare no competing financial interests.

Correspondence should be addressed to Alexander K. Converse at akconverse@wisc.edu.

This paper contains supplemental material available at: https://doi.org/10.1523/JNEUROSCI.0259-25.2025

https://doi.org/10.1523/JNEUROSCI.0259-25.2025

Introduction

Parkinson disease (PD) is a progressive neurodegenerative disorder that affects millions of people globally at great personal and societal cost (Berg et al., 2018; Bloem et al., 2021). While degeneration of dopaminergic cells in the substantia nigra leads to hallmark motor signs of bradykinesia, rigidity, and resting tremor, common treatments that target the dopaminergic system do not fully ameliorate all signs and symptoms of the disease (Seppi et al., 2019). Degeneration of other neurotransmitter systems likely underlies many of the cognitive, autonomic, and other motor signs of PD. It is important, in particular, to better understand the role of the noradrenergic system, which undergoes degeneration early in the course of PD (Delaville et al., 2011; Espay et al., 2014; Paredes-Rodriguez et al., 2020).

The norepinephrine transporter (NET) is located presynaptically on noradrenergic axons, where it controls extracellular neurotransmitter concentrations and is therefore an attractive pharmacological target (Torres et al., 2003). Moreover, measures of NET binding reflect noradrenergic innervation and can serve as an index of neurodegeneration (Tejani-Butt, 1992). Noradrenergic cell bodies are located in the locus coeruleus (LC), where NET may serve within feedback mechanisms to modulate output at downstream terminals (Poe et al., 2020). In PD, NET studies by positron emission tomography (PET) have been limited, but findings include reduced binding of the NET ligand [^{11}C]MeNER in the thalamus (Thal), which highlights a potential central role of noradrenergic degeneration (Nahimi et al., 2018a; Kelberman et al., 2020). Several PET NET radiotracers have been developed in the past for imaging in the CNS, but they generally suffered from poor specificity or selectivity (Ding et al., 2006; Chen et al., 2020). Moreover, there are limited reports of their use for neuroimaging in rats (Schou et al., 2009; Vase et al., 2014). [^{18}F]NS12137 is a recently developed PET radiotracer with high in vitro affinity for NET (K_i ~ 9.5 nM) and good selectivity versus the serotonin (~ 550 nM) and dopamine (~ 650 nM) transporters (Kirjavainen et al., 2018). In rats, both autoradiography and PET indicated high uptake in the NET-rich LC as well as substantial in vivo blockade by the selective NET inhibitor nisoxetine, and no radiometabolites were observed to enter the brain (Kirjavainen et al., 2018;

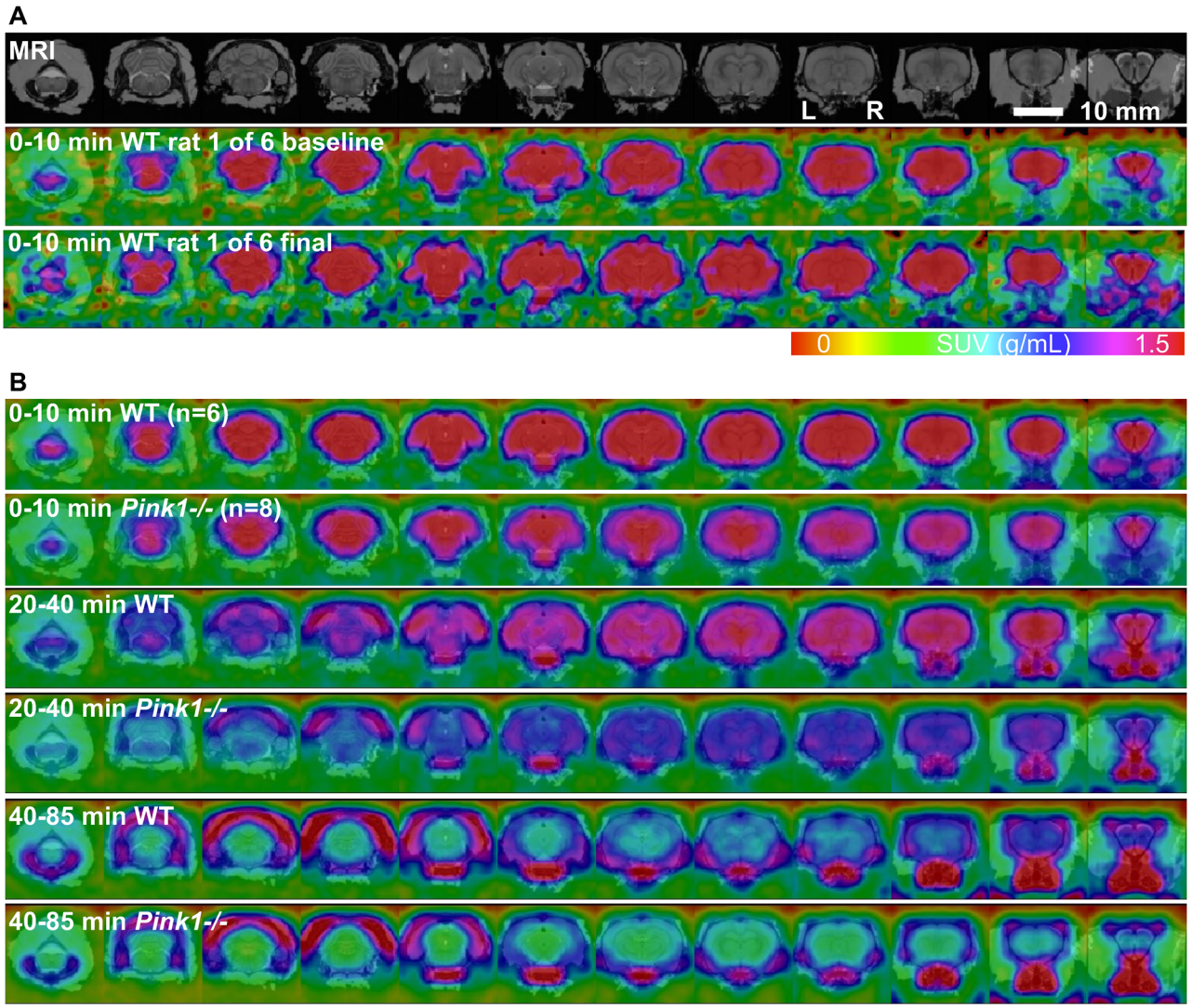

Figure 1. [^{18}F]NS12137 SUV images. Aligned SUV images overlaid on the MRI template. ***A***, Typical examples of 0–10 min SUV images of a single WT subject at baseline and final. ***B***, Average 0–10, 20–40, and 40–85 min SUV images of WT ($n = 6$ at baseline and final) and *Pink1-/-* ($n = 8$ at baseline and final). All SUV images are shown on the 0–1.5 g/ml color scale shown in ***A***. Two millimeters coronal slices, posterior (left) to anterior (right).

Lopez-Picon et al., 2019). [^{18}F]NS12137 is therefore a promising tool for assessing NET within the CNS.

Appropriate animal models of PD are key preclinical research tools. The *Pink1-/-* rat exhibits signs similar to PD, including limb motor deficits, as well as cognitive, cranial sensorimotor, and autonomic dysfunctions (Grant et al., 2015; Cullen et al., 2018; Kelm-Nelson et al., 2021; Krasko et al., 2021, 2023a,b; Rudisch et al., 2023). The *Pink1* gene encodes PTEN-induced putative kinase 1 (PINK1) which facilitates the clearance of defective mitochondria (Pickrell and Youle, 2015; Quinn et al., 2020). In *Pink1-/-* rats, our lab found reduced tyrosine hydroxylase and norepinephrine and increased α_1 receptors in the LC, which is the main site of noradrenergic cell bodies (Kelm-Nelson et al., 2018; Hoffmeister et al., 2021). As in PD (Espay et al., 2014), this suggests that noradrenergic deficits may underly some of the physiological and behavioral abnormalities present in the *Pink1-/-* rat model.

The *Pink1-/-* rat model has previously been studied by MRI and by FDG PET. In MRI scans, *Pink1-/-* rats exhibited abnormal neural activity and reduced white matter integrity in brain regions including Thal and prelimbic area (PrL; Ferris et al., 2018). In recent work by our lab, relative glucose metabolism, as indexed by FDG PET, was found to be lower in *Pink1-/-* rats in several brain regions including PrL (Converse et al., 2024). These findings highlight important differences in *Pink1-/-* rats in basic neurobiological outcomes and point to the need for PD-specific noradrenergic measures.

With an aim toward eventually using [^{18}F]NS12137 to study the effects of interventions on NET in the *Pink1-/-* model, we sought to (1) implement two-tissue compartment reversible tracer pharmacokinetic modeling of [^{18}F]NS12137; (2) validate [^{18}F]NS12137 and analysis methods by comparison with known NET distribution in rat brain, test–retest, and nisoxetine blockade; and (3) characterize NET binding in wild-type (WT) and *Pink1-/-* and test the hypothesis that *Pink1-/-* would exhibit lower binding than WT in LC, PrL, and Thal.

Materials and Methods

Study design

In the main experiment, WT and *Pink1-/-* Long–Evans rats were imaged by PET at two timepoints (baseline and final). Data from these scans were first used to implement pharmacokinetic modeling and to validate methods by comparisons with estimated binding and by test–retest. For further validation, a blockade experiment was performed using a separate group of WT rats that were imaged after pretreatment with the NET ligand nisoxetine. Using the validated methods, [^{18}F]NS12137 binding measures from the main experiment were analyzed in a repeated measures genotype × timepoint design.

Rats

All imaging procedures were approved by the University of Wisconsin-Madison Institutional Animal Care and Use Committee (IACUC protocols G006404, M006390, and M006782) and were conducted in accordance with the Guide for the Care and Use of Laboratory Animals (National Research Council, 2011). Methods and results are reported here according to ARRIVE2.0 guidelines (Percie du Sert et al., 2020). A total of 22 Long–Evans rats (WT $n = 14$ and *Pink1-/-* $n = 8$) were received from Envigo Research Laboratories at 4–6 weeks of age. Genotype was independently confirmed for *Pink1-/-* rats used in this study (Transnetyx). All imaging occurred during the dark period of a 12 h reverse light/dark cycle (12:12). Water and food were provided *ad libitum*. Rats were acclimated to handling and transport before imaging. In the main experiment, six WT male rats were imaged (10.1 ± 0.1 months and 565 ± 65 g at baseline, 12.0 ± 0.1 months and 582 ± 59 g at final) and eight *Pink1-/-* male rats were imaged (9.1 ± 0.1 months and 575 ± 37 g at baseline, 10.7 ± 0.1 months and 575 ± 27 g at final). In the blockade experiment, eight WT rats were imaged (four females 6.0 ± 0.8 months, 267 ± 10 g; four males 6.0 ± 0.8 months, 521 ± 20 g; average ages and weights over three or four scans detailed below.)

Radiotracer

[^{18}F]NS12137 was synthesized generally following methods described previously (Lopez-Picon et al., 2019). Cyclotron-produced (^{18}O(p,n)^{18}F) [^{18}F] fluoride in water was trapped on an anion exchange cartridge (QMA, Waters), which was eluted with Kryptofix 222 (K222, Sigma-Aldrich) solution (10% 0.1 M K222:10% 0.1 M K_2CO_3:80% CH_3CN) into the reaction vial of a semiautomated synthesis unit (CPCU, CTI). The mixture underwent azeotropic distillation at 110°C with four additions of 1.0 ml CH_3CN until dry. NS12137 precursor (2.0 mg in 1.0 ml DMSO, Novandi Chemistry) was added to the dried ^{18}F/K222 and allowed to react for 15 min at 185°C. The reaction vial contents were diluted with 7.0 ml deionized water, trapped on a solid-phase extraction cartridge (tC18 Light, Waters), and eluted into a crude product vial with 0.7 ml tetrahydrofuran. The tetrahydrofuran was dried for 7 min at 80°C under an argon flow to ~0.1 ml. The product was deprotected for 5 min at 80°C with the addition of 0.3 ml HBr (48%) and then neutralized with the addition of 0.8 ml NaOH (3.0 N) and diluted with 1.0 ml HPLC buffer (10 mM K_2PO_4). The crude product vial contents were then injected onto a semipreparative HPLC column (Gemini 5 µm C18 110 Å 250 × 10 mm, Phenomenex) at 4.0 ml/min. The initial mobile phase was 10 mM K_2PO_4 buffer, which was switched to 8% CH_3CN in buffer at 5 min. [^{18}F]NS12137 was collected in 20 ml deionized water at 52 ± 5 min and trapped on a solid-phase extraction cartridge (C18 Light, Waters), which was then rinsed with 20 ml deionized water. The cartridge was eluted with 0.8 ml ethanol through a 0.2 µm filter and followed with 5.0 ml normal saline into a sterile empty vial for injection. A 50 µl sample of the final formulation was injected on an analytic HPLC column using the same mobile phases as the semipreparative method (Gemini 250 × 4.6 mm column, 1.5 ml/min, 0–5 min buffer, 5–40 min 8% CH_3CN, 65% CH_3CN rinse), and the radioactive

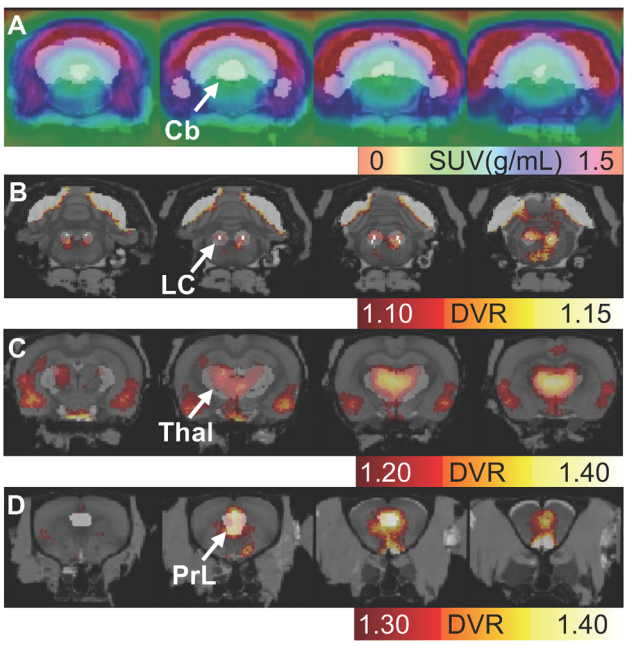

Figure 2. ROIs. ***A***, Cerebellum (Cb, gray, indicated by arrow). Low uptake reference region within the atlas cerebellum (light gray). Overlaid on 40–85 min uptake image (SUV 0–1.5 g/ml). ***B***, LC (gray, indicated by an arrow). Enlargement of original delineation (white dots) to match scanner resolution. Overlaid on binding image (DVR 1.10–1.15). ***C***, Thal (indicated by arrow). High-binding (DVR >1.2) anterior medial portion of the atlas region (gray). Overlaid on a binding image (DVR 1.2–1.4). ***D***, PrL (gray, indicated by an arrow) unchanged from the atlas region. Overlaid on binding image (DVR 1.3–1.4). All [^{18}F]NS12137 SUV and DVR images are averages from six WT at baseline and final. One millimeter coronal slices except LC, which are separated by 0.5 mm; posterior (left) to anterior (right).

peak was observed at 33 ± 2 min, at the same time as standard. Decay corrected yields were 8.7 ± 1.9%, which would likely have been higher using 4 mg precursor (Kirjavainen et al., 2018). Radiochemical purity was >97%. Molar activity at end of synthesis was generally >41 GBq/μmol, although it could not me accurately measured in some of the syntheses (Table S1).

Scans

Scanning was carried out generally as described previously (Converse et al., 2024). Imaging was performed with a microPET P4 tomograph (Siemens) with 2 mm FWHM resolution (Tai et al., 2001). Subjects were positioned up to four at a time parallel to the main axis of the scanner bore under isoflurane anesthesia with head positions fixed by ear and tooth bars. A catheter was placed in a tail vein in each rat. Following a ^{57}Co transmission scan, emission data were collected for 90 min starting with radiotracer injection (target 37 kBq/g). Events were binned into 90 × 1 min sinograms, which were reconstructed with images centered on each rat. Images were corrected for detector sensitivity, deadtime, accidental coincidences, attenuation, scatter, and radioactive decay to yield accurate measures of radioactivity concentration (Bq/mL).

Image alignment, regions of interest, and time-activity curves

Reconstructed images were generally processed as described previously (Converse et al., 2024). To create a well-delineated image of the whole brain, dynamic images were summed over the 10 min following radiotracer injection when delivery peaks. These images were aligned to the Waxholm rat brain atlas (Papp et al., 2014) in an iterative process resulting in the two to four 90 min dynamic images for each animal aligned to each other by 6 degrees of freedom (df) and to the atlas by 9 df. As noted in the Introduction, in this work three brain regions were of interest for NET binding. First, a region in the Waxholm atlas space was delineated for LC with respect to the Paxinos rat atlas (Paxinos and Watson, 1998), which was enlarged to mimic the effect of the finite scanner resolution and better capture signal from this small structure. Second, an anterior medial subregion of Thal was delineated to better capture the high-binding region of [^{18}F]NS12137 and avoid spillover from other brain regions or skull. Third, the Waxholm representation of PrL was used unaltered. Additionally, Cb is a useful reference region for pharmacokinetic modeling because of the low NET concentration found there in histological studies of rats (Kung et al., 2004; Sanders et al., 2005). A subregion of Cb was delineated to avoid spillover from brainstem and skull resulting from the scanner's finite spatial resolution. Time-activity curves (TACs) for these four regions were calculated as standardized uptake values, SUV (g/mL), by dividing the regional radioactivity concentration (Bq/mL) by the injected dose (Bq) per body weight (g).

Pharmacokinetic modeling

For the rats scanned in the main experiment, [^{18}F]NS12137 binding was estimated for each target region (LC, Thal, and PrL) by four measures: (1) mean SUVs were calculated for 40–85 min postinjection of tracer. (2) SUV ratios (SUVr) with respect to Cb were calculated for 40–85 min. (3) Logan graphical method distribution volume ratios (DVR) were calculated with respect to Cb using the slope of the linearized data corresponding to 40–85 min (Logan et al., 1996). (4) Simplified reference tissue method (SRTM) binding potentials with respect to the nondisplaceable compartment (BP_{ND}) were calculated using the Cb reference region and using the 0–85 min TACs (Lammertsma and Hume, 1996). The Logan and SRTM methods are based on the two-tissue compartment model of reversible binding with the outcomes related by $BP_{ND} = DVR - 1$. In evaluating the two-tissue compartment model, which describes transport of the tracer between blood and tissue as well

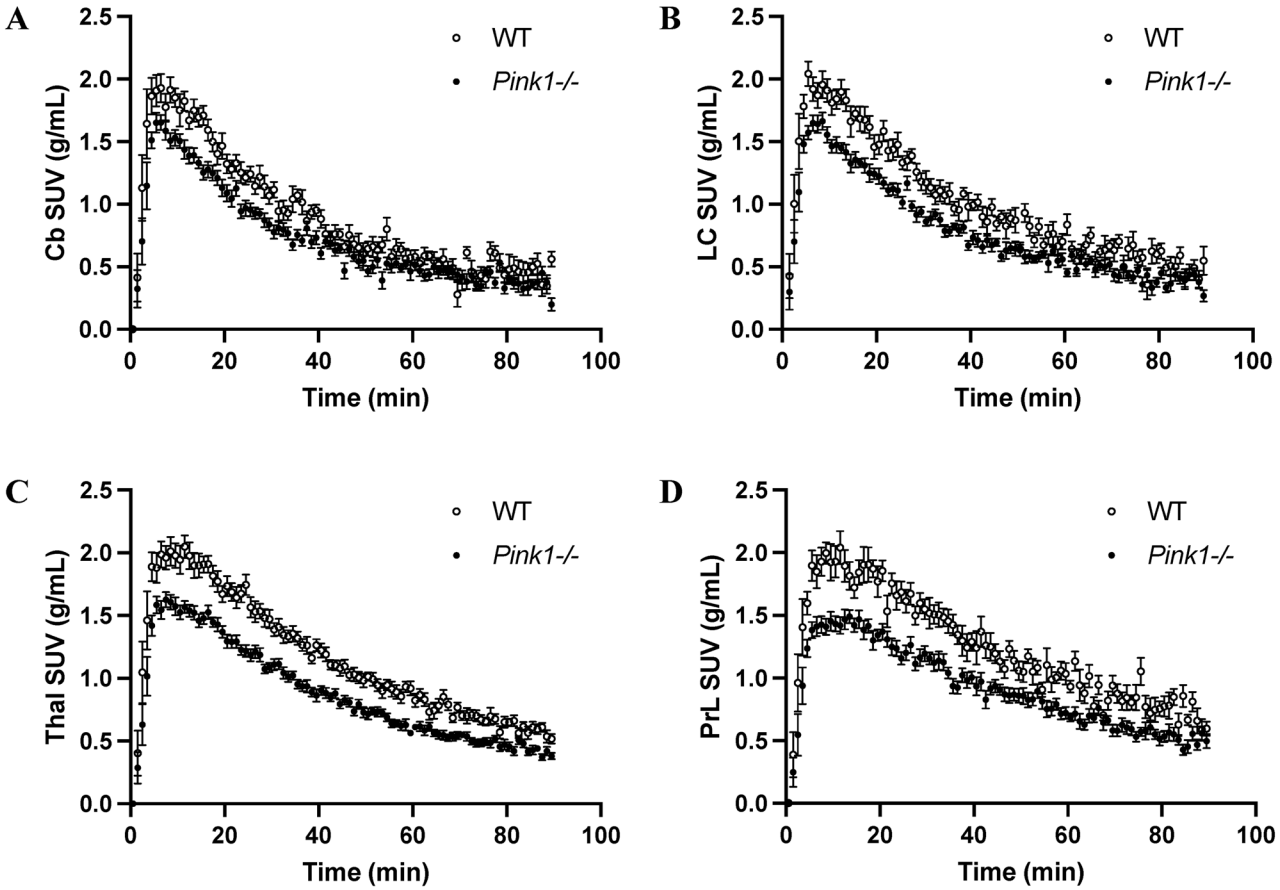

Figure 3. Time course of [^{18}F]NS12137. TACs for (***A***) cerebellum, (***B***) LC, (***C***) Thal, and (***D***) PrL. Points indicate mean ± SEM for WT (open circle; $n = 6$ baseline and final) and *Pink1-/-* (filled circle; $n = 8$ baseline and final).

as binding and release from the target protein within tissue, observed tracer time courses should be followed for long enough to accurately estimate the bound compartment contribution to the PET signal (Innis et al., 2007). In particular, the Logan slope serves as an estimate of the DVR after the ratio of tracer concentrations in the target and reference regions becomes constant (Logan et al., 1996). As described in the Results section, this constant ratio was observed at ~40 min, and therefore the 40–85 min window was chosen for estimates of SUV, SUVr, and Logan DVR. The 0–85 min window was used for the SRTM estimate of BP_{ND}, which utilizes the full time course. As detailed in the Results section, the Logan DVR was chosen as the outcome measure to assess relative NET concentration in LC, Thal, and PrL.

Validation

Estimated binding. The magnitude of [^{18}F]NS12137 binding measured with in vivo PET in the main experiment was compared with that expected based on in vitro measures. The in vivo measure BP_{ND}, binding potential (BP) with respect to the nondisplaceable compartment, is related to the in vitro BP by the free fraction of tracer in the nondisplaceable compartment, $BP_{ND} = f_{ND}\ BP = f_{ND}\ B_{max} / K_d$ (Innis et al., 2007), where the NET concentration in rat Thal is approximately B_{max} = 10 nM (Banay-Schwartz et al., 1992; Sanders et al., 2005; Kanegawa et al., 2012) and the [^{18}F]NS12137 dissociation constant is K_d = 9.5 nM (Kirjavainen et al., 2018). The free fraction, f_{ND}, can be estimated using an inverse power relationship that has been noted between the free fraction of various radiotracers and their lipophilicity P, $1/f_{ND} = 0.43\ P^{0.48}$ (Delforge et al., 1996), where the calculated lipophilicity of [^{18}F]NS12137 is ClogP = 1.58 (Kirjavainen et al., 2018). This leads to an estimate for the in vivo BP of [^{18}F]NS12137 in Thal based on in vitro data of BP_{ND} (estimated) = 0.41.

Test–retest. Within-subject reproducibility of [^{18}F]NS12137 binding (BP_{ND} = DVR − 1) was characterized for WT rats scanned in the main experiment. Reproducibility was measured by percentage test–retest, i.e., 100% × |final − baseline|/baseline (Baumgartner et al., 2018).

Nisoxetine blockade. Prior to radiotracer injection, the rats scanned in the blockade experiment were administered the specific and selective NET ligand nisoxetine (Sigma-Aldrich; Hyttel and Larsen, 1985; Tejani-Butt, 1992). In a crossover design, rats were imaged after administration of 0, 5, and 10 mg/kg racemic nisoxetine. Four of the eight rats (two females) were subsequently scanned at 20 mg/kg. Nisoxetine was administered 30 min prior to radiotracer by bolus intravenous injection in 1.0 ml saline under isoflurane anesthesia. In the first scan session, in which one rat was scanned at 0 and one at 5 mg/kg, the heart rate was observed to rapidly decline upon injection in the rat receiving nisoxetine. To improve tolerance for the drug in subsequent sessions, the dose was administered in five boluses of 0.2 ml evenly separated over 5 min (ten minutes at 20 mg/kg). Each rat's scans were separated by at least 2 weeks.

Effects of genotype and time

To examine the effects of genotype and time, binding measures from the main experiment were analyzed in a 2 (WT and *Pink1-/-*) × 2 (baseline and final) repeated measures design.

Statistical analysis

Correlations across rats between binding estimation methods were analyzed by Pearson's *r*, nisoxetine effects at 0 and 5 mg/kg were analyzed by paired *t* test, sex effects were analyzed by two-sample *t* test, and genotype × time effects were analyzed by two-way repeated–measure ANOVA, all with significance set at $\alpha = 0.05$. Analyses were performed using GraphPad Prism (version 10.2.3). To qualitatively confirm genotype differences in [^{18}F]NS12137 binding found in the genotype × time region of interest (ROI) analysis, a voxelwise two-sample *t* test of *Pink1-/-* versus WT images was generated and arbitrarily thresholded at $|t| > 0.5$.

Results

As detailed below, the PET images revealed a pattern of elevated [^{18}F]NS12137 binding in regions with known high concentrations of NET, including LC, Thal, and PrL. Reproducible estimates of [^{18}F]NS12137 binding were obtained with the Logan linearized version of the two-tissue compartment pharmacokinetic model using a cerebellar reference region. Pretreatment with the NET ligand nisoxetine (5 mg/kg) substantially reduced [^{18}F]NS12137 binding. In a comparison of WT and *Pink1-/-* rats, reduced [^{18}F]NS12137 binding was observed in Thal and PrL.

Image alignment and TACs

Aligned images agreed with the outline of the brain atlas to better than 0.5 mm, which is sufficient for accurate identification of ROIs (Fig. 1). [^{18}F]NS12137 uptake was lowest in Cb early in the radiotracer time course, and a cerebellar subregion was created that avoided radioactivity spillover from the skull at later times (Fig. 2*A*). The LC ROI was enlarged to match the scanner resolution and better capture signal from this small structure (Fig. 2*B*). A ROI was delineated on the anterior medial portion of Thal where binding was high (Fig. 2C). The atlas PrL region closely matched the region of highest binding in the frontal cortex (Fig. 2*D*). Average TACs for these four regions (Cb, LC, Thal,

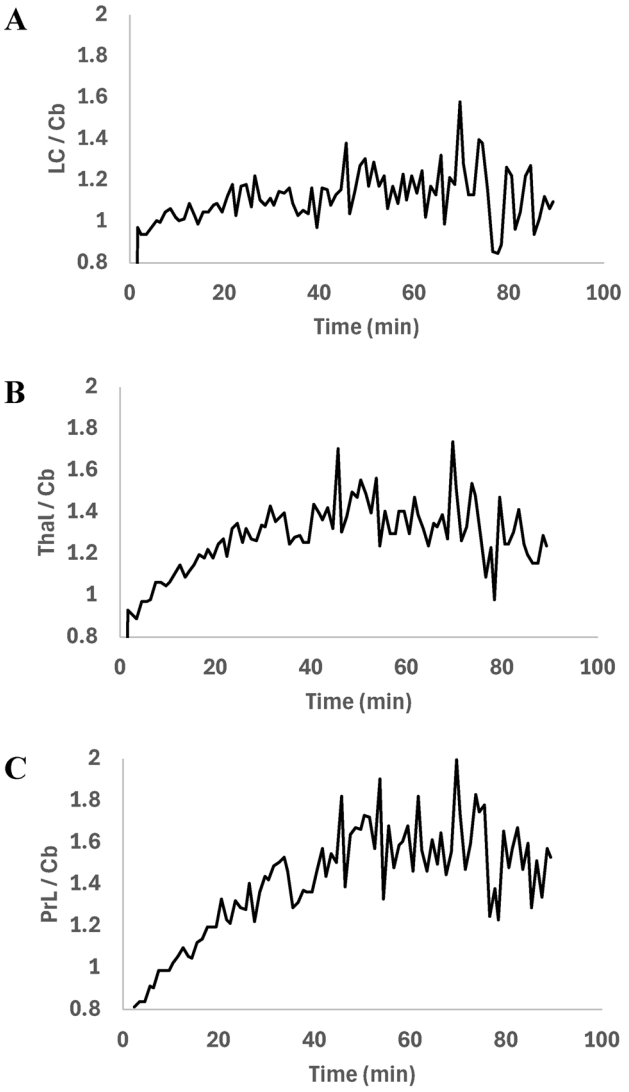

Figure 4. Target to the reference region ratio. The ratio of target to cerebellar reference region [^{18}F]NS12137 radioactivity concentrations rises until ~40 min in (***A***) LC, (***B***) Thal, and (***C***) PrL. The approximately constant ratio thereafter satisfies an assumption of the Logan reference region method. Ratio of average target region and cerebellar TACs ($n = 6$ WT baseline and final; $n = 8$ *Pink1-/-* baseline and final).

and PrL) are shown in Figure 3, and individual aligned images and TACs are shown in Figure S1.

Pharmacokinetic modeling

The ratio of tracer concentration in the target region to that in the reference region became constant at ~40 min (Fig. 4). The target to reference region DVRs were therefore estimated using the Logan slope from 40 to 85 min. Typical Logan and SRTM fits are shown in Figure 5. Comparisons of binding estimates from the four methods, SUV, SUVr, Logan, and SRTM, are shown in Figure 6. In general, SUV can be sensitive to differences in absorption, distribution, metabolism, and excretion (ADME), SUVr can be sensitive to regional differences in blood flow, and SRTM may be subject to sporadic outliers. Therefore, binding estimates were calculated using the Logan method, which is insensitive to variability in ADME, accounts for differences in regional tracer delivery and efflux, and is computationally simple.

Validation

Estimated binding

Based on in vitro data, the estimated BP in Thal with respect to the nondisplaceable compartment was BP_{ND} (estimated) = 0.41. In comparison, the observed value was $BP_{ND} = DVR - 1 = 0.29 \pm 0.04$ (mean ± SEM; $n = 6$ WT males at baseline).

Test–retest

The percentage test–retest (100% × |final−baseline|/baseline) of [^{18}F]NS12137 binding ($BP_{ND} = DVR - 1$) in the three target regions was 37 ± 32% in LC, 34 ± 21% in Thal, and 31 ± 16% in PrL (mean ± SD; six WT males).

Nisoxetine blockade

Pretreatment with 5 mg/kg nisoxetine (Tejani-Butt, 1992) significantly reduced [^{18}F]NS12137 binding in LC (Fig. 7; $p = 0.016$; paired t test; $n = 6$ WT; three males and three females). Of eight rats scanned at both 0 and 5 mg/kg, one was excluded because the intravenous line failed for the 5 mg/kg scan, and a second was excluded because the nisoxetine was given in a single bolus, which resulted in a noticeable change in the heart rate and a paradoxical large increase in apparent binding. Scans following administration of 10 and 20 mg/kg nisoxetine did not exhibit reduced [^{18}F]NS12137 binding (Figs. S3*A*,*C*,*E*, S4). At these higher doses, the heart rate was altered by the nisoxetine administration, and, notably, [^{18}F]NS12137 uptake increased in a dose-dependent manner in all regions including the reference region (Fig. S3*B*,*D*,*F*,*G*). No significant effect of sex was observed on [^{18}F]NS12137 binding in LC, Thal, or PrL at 0 mg/kg nisoxetine (p's > 0.16; two-sample t test; $n = 6$ WT; three males and three females).

Effects of genotype and time

No significant interaction of genotype and time was observed in LC ($p = 0.40$; six WT and eight *Pink1-/-* males), Thal ($p = 0.85$),

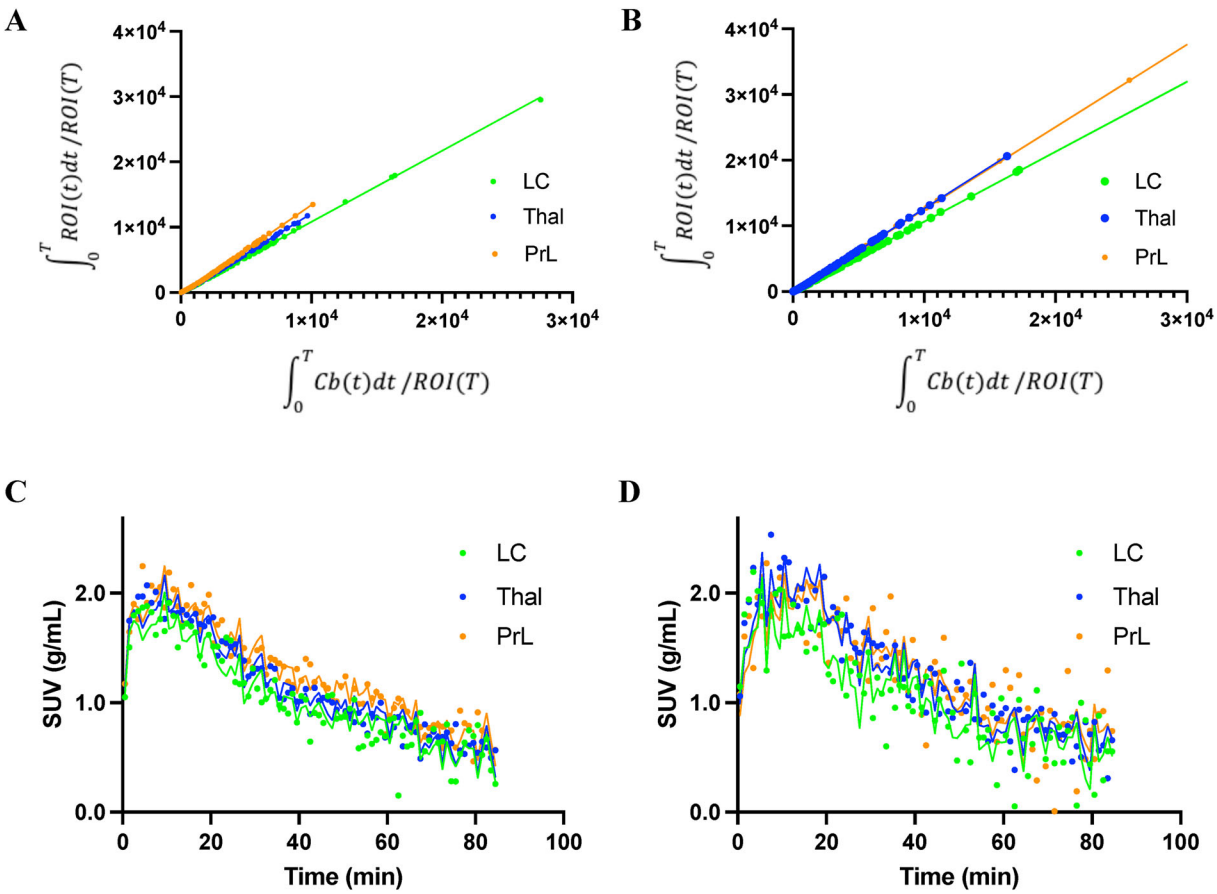

Figure 5. Pharmacokinetic model fits to data. Examples from one WT rat of two-tissue compartmental model fits to time courses for three ROIs. ***A***, Baseline and (***B***) final Logan graphical method fits. The corresponding (***C***) baseline and (***D***) final simplified reference tissue model (SRTM) fits. LC, locus coeruleus; Thal, thalamus; PrL, prelimbic area. Both models use a cerebellar (Cb) reference region. The Logan DVR and SRTM BP with respect to the nondisplaceable compartment (BP_{ND}) are mathematically related as $DVR = BP_{ND} + 1$. In this rat, the best fit model parameters at baseline were LC, DVR = 1.087 and $BP_{ND} = 0.127$; Thal, 1.237 and 0.240; and PrL, 1.379 and 0.399, and at final they were LC, 1.065 and 0.088; Thal, 1.273 and 0.287; and PrL, 1.255 and 0.305.

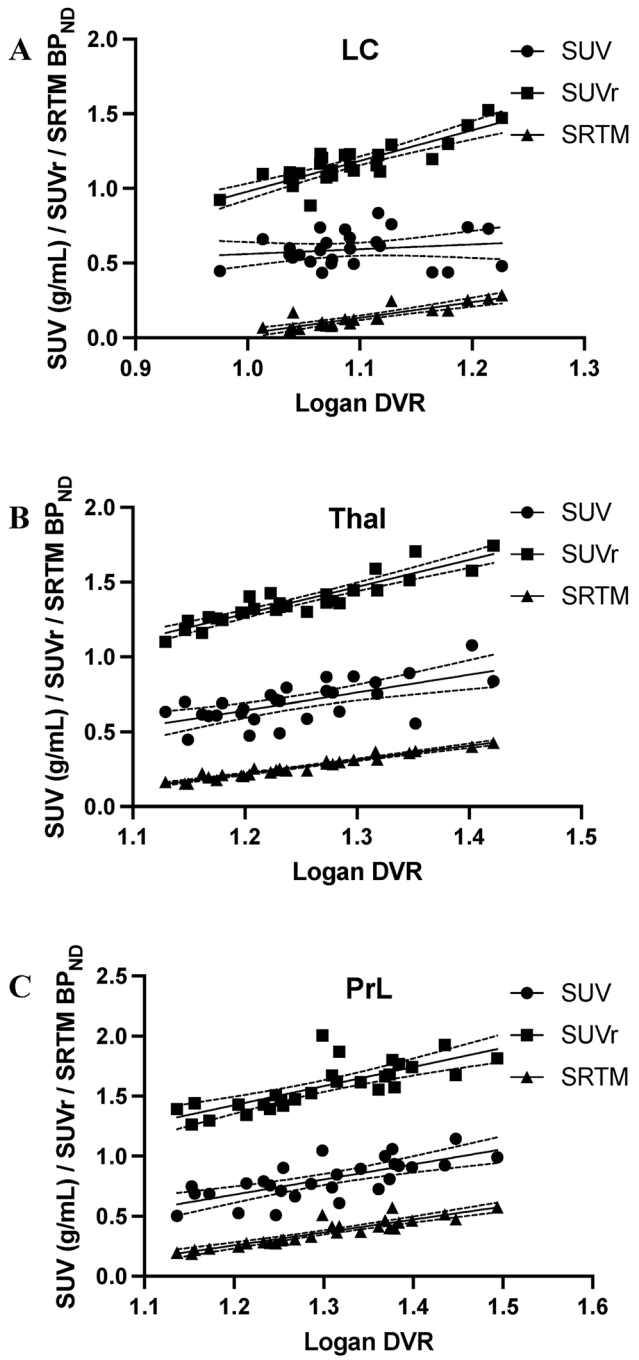

Figure 6. Comparison of binding estimation methods. SUV, SUV relative to the cerebellum (SUVr), and simplified reference tissue model (SRTM) BP (BP_{ND}) plotted against Logan DVR. SRTM agrees best with Logan, followed by SUVr, and then SUV. Pearson's correlation coefficients are as follows: (***A***) LC, SUV $r = 0.17$; SUVr $r = 0.86$; SRTM $r = 0.88$; (***B***) Thal, SUV $r = 0.64$; SUVr $r = 0.92$; SRTM $r = 0.97$; (***C***) PrL, SUV $r = 0.71$; SUVr $r = 0.78$; SRTM $r = 0.92$. Logan DVR, SUV, and SUVr were calculated using 40–85 min data and SRTM using 0–85 min. Results from 14 pairs of scans are plotted ($n = 6$ WT and $n = 8$ *Pink1-/-* males at the baseline and final) except for the SRTM estimate of LC binding, for which five outliers were excluded with $BP_{ND} > 0.3$.

or PrL ($p = 0.39$). Main effects of genotype were observed such that [^{18}F]NS12137 binding was lower in *Pink1-/-* compared with WT in Thal ($p = 0.0059$) and PrL ($p = 0.014$) (Fig. 8) but not in LC ($p = 0.30$). No main effect of time was observed in LC ($p = 0.78$), Thal ($p = 0.39$), or PrL ($p = 0.34$). These ROI results are detailed in Table 1 and qualitatively confirmed by voxelwise binding maps shown in Figure 9. Individual measures are provided in Table S1 and Figures S1 and S2.

Discussion

In this work, we (1) implemented two-tissue compartment reversible tracer pharmacokinetic modeling of [^{18}F]NS12137 in the rat brain with the Logan reference tissue method; (2) validated [^{18}F]NS12137 PET neuroimaging and analysis methods by comparison with known NET densities, test–retest, and nisoxetine blockade; and (3) found reduced [^{18}F]NS12137 binding in the *Pink1-/-* rat model of PD compared with WT controls in Thal and PrL.

Pharmacokinetic modeling

We implemented two-tissue compartment pharmacokinetic models to estimate binding parameters from the observed [^{18}F]NS12137 PET time courses in rats using a reference region with negligible target protein concentration (Logan et al., 2005). Across species and tracers, the striatum and cerebellum have generally exhibited low NET expression; in particular, radiolabeled nisoxetine binding in rats has been reported to be similarly low in the cerebellum and striatum (Kung et al., 2004; Sanders et al., 2005). In the present study, cerebellum exhibited the lowest [^{18}F]NS12137 uptake of all regions examined, and we therefore used it as the reference region. Skull uptake of radioactivity was observed in the later portion of the radiotracer time course likely due to [^{18}F]fluoride released by peripheral defluorination of [^{18}F]NS12137 (Lopez-Picon et al., 2019), and this necessitated careful delineation of the Cb reference region. The time course of the ratio of the [^{18}F]NS12137 concentration in the target region versus Cb reached a plateau, which is a prerequisite for taking the Logan slope alone as an estimate of the DVR (Logan et al., 1996).

The Logan method is in principle superior to SUV and SUVr because SUV is sensitive to variation in ADME and SUVr reflects differences between the target and reference regions in tracer delivery and efflux. The Logan and SRTM methods are based on the two-tissue compartment model, and they are insensitive to variations in ADME as well as differences in blood flow between target and reference regions. While Logan uses a two-parameter linear fit, SRTM requires a three-parameter nonlinear fit. The nonlinear fitting algorithm used here (Kennedy and Eberhart, 1995) is designed to sample the full extent of the model parameter space; however it occasionally converged on local minima of the least squares cost function and incorrectly estimated the SRTM BP. This resulted in some outliers for LC, likely due to noisier TACs from this small region. We therefore chose the Logan method to estimate [^{18}F]NS12137 binding. Nevertheless, it is reassuring that the Logan and SRTM results otherwise agreed well, despite the different approximations and computational pathways involved.

Validation

Estimated binding

Our in vivo PET measure of the [^{18}F]NS12137 BP in Thal is in agreement with the estimated BP based on reported in vitro measures. Also, in agreement with histology studies of NET concentration reported in the literature, we observed elevated [^{18}F]NS12137 binding in LC, Thal, and PrL. These regions have been identified in rats as having high concentrations of NET by [^{3}H]nisoxetine autoradiography (Tejani-Butt, 1992; Sanders et al., 2005; Kanegawa et al., 2012), 2-[^{125}I]iodo-nisoxetine autoradiography (Kung et al., 2004), and immunohistochemistry

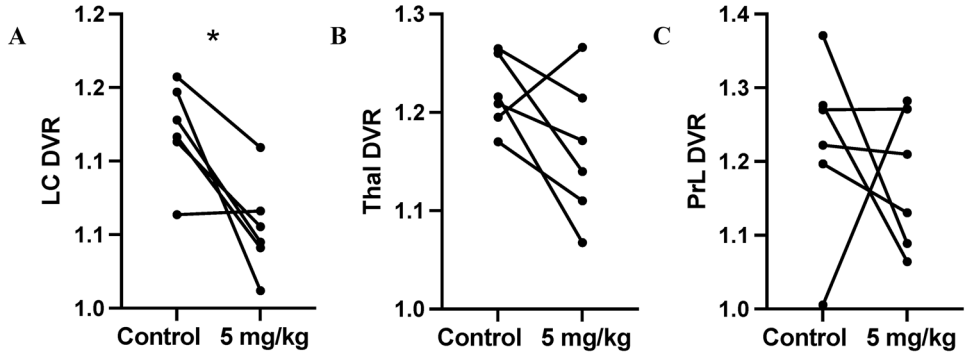

Figure 7. Nisoxetine blockade. [^{18}F]NS12137 DVR in WT rats pretreated with nisoxetine (5 mg/kg) or saline. ***A***, LC exhibited a 56% reduction in average binding (BP_{ND} = DVR − 1; $p = 0.016$), (***B***) Thal n.s. and (***C***) the prelimbic cortex n.s. (paired *t* test; $n = 6$; 3 males and 3 females). One rat exhibited higher binding at 5 mg/kg compared with control in all three regions. Missing data from two rats is described in the text.

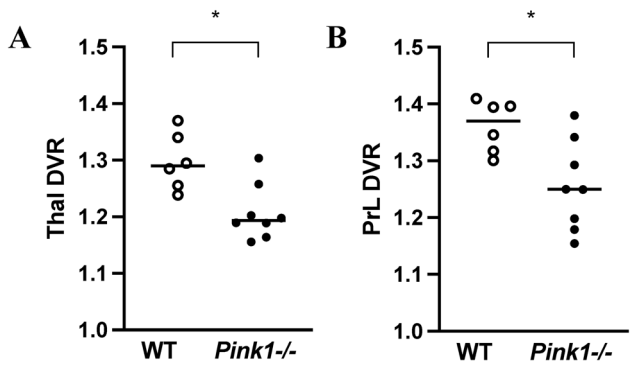

Figure 8. Genotype differences in [^{18}F]NS12137 binding. Reduced binding was observed in *Pink1-/-* versus WT in (***A***) Thal ($p = 0.0059$) and (***B***) PrL ($p = 0.014$). Main effect of genotype in genotype × time ANOVA; mean DVR over the baseline and final is plotted for each rat ($n = 6$ WT males and $n = 8$ *Pink1-/-* males).

with the 43411 antibody and optical microscopy (Schroeter et al., 2000). Additionally, NET in PrL has been characterized by the 43411 antibody with electron microscopy (Miner et al., 2003). While histological methods provide spatial resolution under 0.01 mm, PET is limited to ∼2 mm. Hence, regions with high reported densities of NET, namely, LC and anteroventral thalamic nucleus, are expected to display modest average [^{18}F]NS12137 binding with PET because of their small size. Moreover, other regions of known high NET concentration, e.g., the hypothalamus and insular cortex, exhibited elevated [^{18}F]NS12137 binding, but we chose not to analyze them due to their nearness to contaminating radioactivity in skull especially at later times. These regions may, however, be amenable to quantification by [^{18}F]NS12137 PET with suitable anatomical delineation and using earlier times. Additionally, much NET, at least in PrL, is apparently located within the cell plasma and not bound in the cell membrane (Miner et al., 2003). Therefore, if NS12137 could be fluorescently labeled, it would be interesting to examine the subcellular location of the bound molecules by microscopy (Richardson et al., 2016).

Test–retest

Moderate percentage test–retest measures were observed, as might be expected given the small region volumes and relatively low-binding values.

Nisoxetine blockade

Nisoxetine blockade at 5 mg/kg yielded a reduction of binding in LC, in line with reports of nisoxetine blockade studies in rats with [^{18}F]NS12137 (Kirjavainen et al., 2018; Lopez-Picon et al., 2019) as well as 2-[^{125}I]iodo-nisoxetine (Kung et al., 2004). However, at higher nisoxetine doses of 10 and 20 mg/kg, we were surprised to find no reduction in [^{18}F]NS12137 binding. We observed acute reductions in the heart rate with intravenous injections of nisoxetine, and significant reductions in blood pressure in rats have been reported 1 h after administration of 10 and 30 mg/kg nisoxetine, but not 3 mg/kg (Bello et al., 2013). We additionally noted a nisoxetine dose-dependent increase in [^{18}F]NS12137 SUV in LC, Thal, PrL, and Cb. This may have been due to blockade of peripheral binding sites resulting in higher concentration of radiotracer in the blood. Perhaps it was due in part to hemodynamic changes yielding increased delivery and/or reduced washout of [^{18}F]NS12137 at 10 and 20 mg/kg nisoxetine. A dose-dependent hemodynamic response to nisoxetine may have caused time-varying brain blood flow patterns over the course of the PET scan, leading to inaccurate estimates of [^{18}F]NS12137 binding at 10 and 20 mg/kg. While the in vitro binding profile of NS12137 is very good, further work may be warranted to confirm the in vivo specificity and selectivity of [^{18}F]NS12137 (Kirjavainen et al., 2018; Lopez-Picon et al., 2019).

Effects of genotype and time

We observed a 30% reduction in [^{18}F]NS12137 binding in *Pink1-/-* compared with that in WT rats in both Thal and PrL. To our knowledge, this is the first reported evidence of reduced NET expression in the *Pink1-/-* model. This observation is in line with immunohistochemical studies from our lab of other noradrenergic abnormalities in *Pink1-/-*, namely, reduced tyrosine hydroxylase and norepinephrine, and increased α_1 receptors in LC (Kelm-Nelson et al., 2018; Hoffmeister et al., 2021). Reduced NET binding in Thal observed here in *Pink1-/-* rats and in PET studies of PD (Sommerauer et al., 2018; Nahimi et al., 2018b) could reflect diminished noradrenergic projections from LC, which in PD are implicated in nonmotor symptoms including impaired wakefulness, disrupted sleep–wake cycle, depression, and anxiety (Espay et al., 2014). Similarly, neurodegeneration of LC axons may be responsible for the reduced NET binding we observed in *Pink1-/-* rats in PrL. Moreover, in a recent [^{18}F]fluorodeoxyglucose PET study, we observed lower uptake in PrL in *Pink1-/-* rats compared with that in WT (Converse et al., 2024). Perhaps reduced glucose metabolism in

Table 1. Genotype and time effects on [^{18}F]NS12137 binding

	Mean ± SEM									
	Baseline		Final		Genotype × time		Genotype		Time	
	WT	*Pink1-/-*	WT	*Pink1-/-*	$F_{1,12}$	*p*	$F_{1,12}$	*p*	$F_{1,12}$	*p*
n	6	8	6	8						
Age (mon)	10.00 ± 0.05	9.12 ± 0.05	12.04 ± 0.05	10.74 ± 0.02						
Weight (g)	565 ± 27	575 ± 13	582 ± 24	575 ± 9						
LC DVR	1.120 ± 0.020	1.073 ± 0.016	1.093 ± 0.027	1.087 ± 0.027	0.78	0.40	1.20	0.30	0.08	0.78
Thal DVR	1.290 ± 0.041	1.195 ± 0.013	1.305 ± 0.011	1.220 ± 0.026	0.04	0.85	11.18	0.006**	0.80	0.39
PrL DVR	1.384 ± 0.039	1.257 ± 0.034	1.337 ± 0.021	1.254 ± 0.026	0.80	0.39	8.35	0.014*	0.97	0.34

*$p < 0.05$; **$p < 0.01$ repeated-measure ANOVA. LC, locus coeruleus; Thal, thalamus; PrL, prelimbic area; DVR, distribution volume ratio.

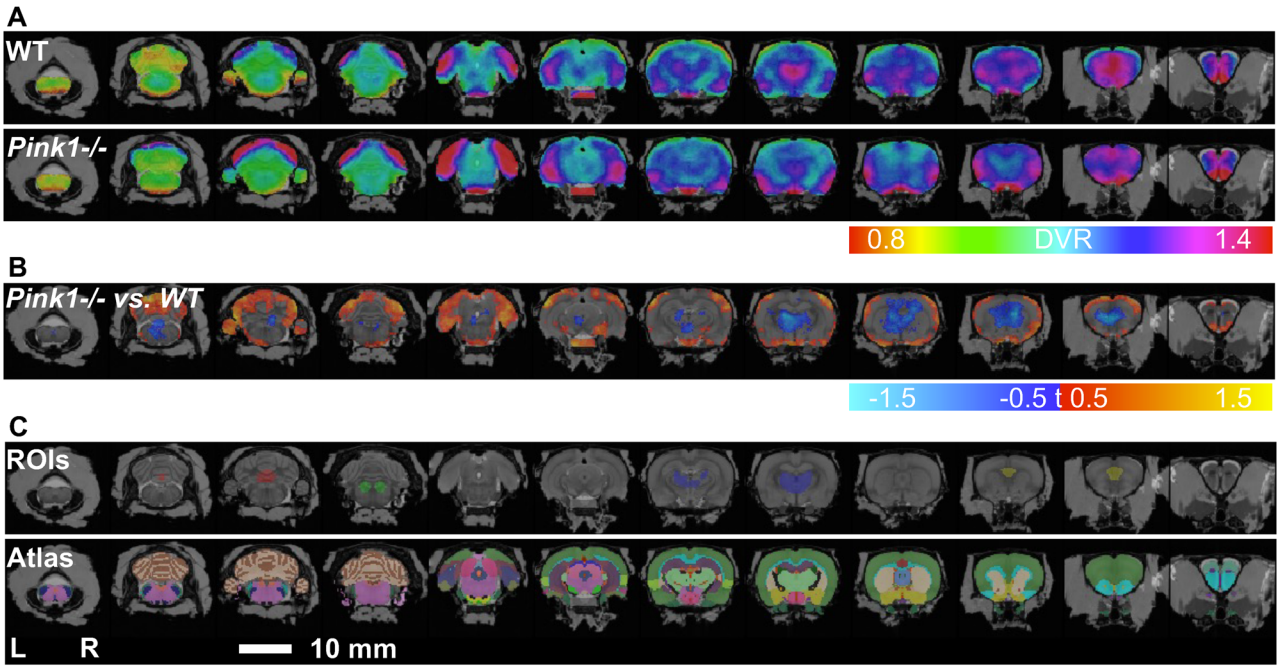

Figure 9. [^{18}F]NS12137 binding images. ***A***, Voxelwise maps of average [^{18}F]NS12137 binding. Two millimeters coronal slices overlaid on an MRI template. Elevated binding is apparent in Thal and PrL. DVR with respect to the cerebellar reference region is shown for WT ($n = 6$ baseline and final) and *Pink1-/-* rats ($n = 8$ baseline and final). ***B***, Comparison of *Pink1-/-* and WT binding. Voxelwise two-sample *t* test thresholded at $|t|>0.5$. Red indicates voxels with higher binding in *Pink1-/-* compared with WT, and blue indicates lower binding. Reduced binding in *Pink1-/-* in Thal and PrL qualitatively confirms ROI analyses. Some differences near edge of the brain may be artifacts of skull uptake from peripheral radiotracer defluorination. ***C***, ROIs used in main analysis: red, cerebellar reference region (Cb); green, LC; blue, Thal; and yellow, prelimbic area (PrL). The Waxholm atlas parcellation is shown for reference (Papp et al., 2014).

PrL in *Pink1-/-* rats is due to reduced noradrenergic innervation. PrL is thought to be homologous to human dorsolateral prefrontal cortex (dlPFC), which is of interest in PD as it may be responsible for associated difficulties with working memory and attention (Vertes, 2004; Espay et al., 2014; Randver, 2018; De Bartolo et al., 2025). Regarding norepinephrine in this region, lesions of noradrenergic afferents to PrL in rats resulted in attentional deficits (Newman et al., 2019), and, in an fMRI study of PD patients, dlPFC connectivity was found to be reduced compared with controls, while inhibition of NET by atomoxetine in the PD subjects led to alterations in dlPFC connectivity that correlated positively with changes in verbal fluency (Borchert et al., 2016).

We did not observe a genotype difference in NET binding in LC, which is consistent with previous immunohistochemistry work from our lab that found no difference between *Pink1-/-* and WT rats in NET in LC (Hoffmeister et al., 2021). In the present study, any genotype difference in LC may have been obscured by the low binding observed in this small structure due to the 2 mm PET resolution. On the other hand, it is interesting to note that in PET PD studies, LC did not show as robust a reduction in NET binding as Thal (Nahimi et al., 2018a). Perhaps compensatory or protective mechanisms at work in *Pink1-/-* rats and PD help maintain NET expression in LC.

Regarding neurodegeneration, we did not observe a genotype × time interaction in LC, Thal, or PrL, but it may be that the time between the baseline and final timepoints was too short. Nevertheless, the detection of genotype differences in [^{18}F]NS12137 binding suggests that it may be possible to observe altered neurodegeneration in *Pink1-/-* rats in response to interventions using a long enough time window.

Limitations

As detailed above, this study was subject to certain limitations. The blockade experiment was inconclusive at higher doses, perhaps because the binding estimation was compromised by cardiovascular effects associated with intravenous injection of nisoxetine. In the main experiment, the age window examined may have been too narrow to observe neurodegeneration in the

Pink1-/- rats compared with WT. Additionally, given sex differences in PD (Gillies et al., 2014), the noradrenergic system (Bangasser et al., 2016), and the *Pink1-/-* rat model (Marquis et al., 2020; Lechner et al., 2022), it is important to study both sexes. As part of our lab's increasing efforts to include female rats, they were studied in the blockade experiment. Logistical issues prevented us from studying females in the main experiment. Finally, in the main experiment, in 18 rat scans we estimated upper limits on occupancy by NS12137 of $<4 \pm 2\%$ (Table S1). For the other 10 rat scans, the radiosynthesis analytical HPLC mass detection limit was high due to technical difficulties, and the occupancy limits were therefore high. In these 10 scans, however, the observed binding appears unaffected, consistent with negligible NS12137 mass present in the radiotracer.

Conclusions

[^{18}F]NS12137 binding provides a reproducible and specific measure that indicates reduced NET in *Pink1-/-* rats. Noninvasive in vivo [^{18}F]NS12137 PET imaging is therefore a promising method for the study of potential therapies in the *Pink1-/-* rat model of PD.

References

Banay-Schwartz M, Kenessey A, DeGuzman T, Lajtha A, Palkovits M (1992) Protein content of various regions of rat brain and adult and aging human brain. Age (Omaha) 15:51–54.

Bangasser DA, Wiersielis KR, Khantsis S (2016) Sex differences in the locus coeruleus-norepinephrine system and its regulation by stress. Brain Res 1641:177–188.

Baumgartner R, Joshi A, Feng D, Zanderigo F, Ogden RT (2018) Statistical evaluation of test-retest studies in PET brain imaging. EJNMMI Res 8:13.

Bello NT, Walters AL, Verpeut JL, Cunha PP (2013) High-fat diet-induced alterations in the feeding suppression of low-dose nisoxetine, a selective norepinephrine reuptake inhibitor. J Obes 2013:457047.

Berg D, et al. (2018) Movement disorder society criteria for clinically established early Parkinson's disease. Mov Disord 33:1643–1646.

Bloem BR, Okun MS, Klein C (2021) Parkinson's disease. Lancet 397:2284–2303.

Borchert RJ, et al. (2016) Atomoxetine enhances connectivity of prefrontal networks in Parkinson's disease. Neuropsychopharmacology 41:2171–2177.

Chen X, Kudo T, Lapa C, Buck A, Higuchi T (2020) Recent advances in radiotracers targeting norepinephrine transporter: structural development and radiolabeling improvements. J Neural Transm 127:851–873.

Converse AK, et al. (2024) Positron emission tomography neuroimaging of [^{18}F]fluorodeoxyglucose uptake and related behavior in the Pink1-/- rat model of Parkinson disease. Front Neurosci 18:1–18.

Cullen KP, Grant LM, Kelm-Nelson CA, Brauer AFL, Bickelhaupt LB, Russell JA, Ciucci MR (2018) Pink1 -/- rats show early-onset swallowing deficits and correlative brainstem pathology. Dysphagia 33:749–758.

De Bartolo MI, et al. (2025) Association of early fMRI connectivity alterations with different cognitive phenotypes in patients with newly diagnosed Parkinson disease. Neurology 104:e210192.

Delaville C, De Deurwaerdère P, Benazzouz A (2011) Noradrenaline and parkinson's disease. Front Syst Neurosci 5:31.

Delforge J, Syrota A, Bendriem B (1996) Concept of reaction volume in the in vivo ligand-receptor model. J Nucl Med 37:118–125.

Ding YS, Lin K-S, Logan J (2006) PET imaging of norepinephrine transporters. Curr Pharm Des 12:3831–3845.

Espay AJ, LeWitt PA, Kaufmann H (2014) Norepinephrine deficiency in Parkinson's disease: the case for noradrenergic enhancement. Mov Disord 29:1710–1719.

Ferris CF, Morrison TR, Iriah S, Malmberg S, Kulkarni P, Hartner JC, Trivedi M (2018) Evidence of neurobiological changes in the presymptomatic PINK1 knockout rat. J Parkinsons Dis 8:281–301.

Gillies GE, Pienaar IS, Vohra S, Qamhawi Z (2014) Sex differences in Parkinson's disease. Front Neuroendocrinol 35:370–384.

Grant LM, Kelm-Nelson CA, Hilby BL, Blue KV, Paul Rajamanickam ES, Pultorak JD, Fleming SM, Ciucci MR (2015) Evidence for early and progressive ultrasonic vocalization and oromotor deficits in a PINK1 gene knockout rat model of Parkinson's disease. J Neurosci Res 93:1713–1727.

Hoffmeister JD, Kelm-Nelson CA, Ciucci MR (2021) Quantification of brainstem norepinephrine relative to vocal impairment and anxiety in the Pink1-/- rat model of Parkinson disease. Behav Brain Res 414:113514.

Hyttel J, Larsen JJ (1985) Neurochemical profile of Lu 19-005, a potent inhibitor of uptake of dopamine, noradrenaline, and serotonin. J Neurochem 44:1615–1622.

Innis RB, et al. (2007) Consensus nomenclature for in vivo imaging of reversibly binding radioligands. J Cereb Blood Flow Metab 27:1533–1539.

Kanegawa N, Kiyono Y, Sugitaa T, Kuge Y, Fujibayasi Y, Saji H (2012) Norepinephrine transporter imaging in the brain of a rat model of depression using radioiodinated (2S, αS)-2-(α-(2-iodophenoxy)benzyl)morpholine. Mol Imaging 11:280–285.

Kelberman M, Keilholz S, Weinshenker D (2020) What's that (blue) spot on my MRI? Multimodal neuroimaging of the locus coeruleus in neurodegenerative disease. Front Neurosci 14:583421.

Kelm-Nelson CA, Trevino MA, Ciucci MR (2018) Quantitative analysis of catecholamines in the Pink1 -/- rat model of early-onset Parkinson's disease. Neuroscience 379:126–141.

Kelm-Nelson CA, Lechner SA, Lettenberger SE, Kaldenberg TAR, Pahapill NK, Regenbaum A, Ciucci MR (2021) Pink1(-/-) rats are a useful tool to study early Parkinson disease. Brain Commun 3:fcab077.

Kennedy J, Eberhart R (1995) Particle swarm optimization. In: 1995 ieee international conference on neural networks proceedings, VOLS 1-6, pp 1942–1948.

Kirjavainen AK, Forsback S, Lopez-Picon FR, Marjamaki P, Takkinen J, Haaparanta-Solin M, Peters D, Solin O (2018) ^{18}F-labeled norepinephrine transporter tracer [^{18}F]NS12137: radiosynthesis and preclinical evaluation. Nucl Med Biol 56:39–46.

Krasko MN, Hoffmeister JD, Schaen-Heacock NE, Welsch JM, Kelm-Nelson CA, Ciucci MR (2021) Rat models of vocal deficits in Parkinson's disease. Brain Sci 11:1–21.

Krasko MN, Rudisch DM, Burdick RJ, Schaen-Heacock NE, Broadfoot CK, Nisbet AF, Rogus-Pulia N, Ciucci MR (2023a) Dysphagia in Parkinson disease: part II—current treatment options and insights from animal research. Curr Phys Med Rehabil Rep 11:188–198.

Krasko MN, Szot J, Lungova K, Rowe LM, Leverson G, Kelm-Nelson CA, Ciucci MR (2023b) Pink1-/- rats demonstrate swallowing and gastrointestinal dysfunction in a model of prodromal Parkinson disease. Dysphagia 38:1382–1397.

Kung MP, Choi S-R, Hou C, Zhuang Z-P, Foulon C, Kung HF (2004) Selective binding of 2-[^{125}I]iodo-nisoxetine to norepinephrine transporters in the brain. Nucl Med Biol 31:533–541.

Lammertsma AA, Hume SP (1996) Simplified reference tissue model for PET receptor studies. Neuroimage 4:153–158.

Lechner SA, Welsch JM, Pahapill NK, Kaldenberg TAR, Regenbaum A, Kelm-Nelson CA (2022) Predictors of prodromal Parkinson's disease in young adult Pink1-/- rats. Front Behav Neurosci 16:867958.

Logan J, Fowler JS, Volkow ND, Wang GJ, Ding YS, Alexoff DL (1996) Distribution volume ratios without blood sampling from graphical analysis of PET data. J Cereb Blood Flow Metab 16:834–840.

Logan J, Ding Y-S, Lin K-S, Pareto D, Fowler J, Biegon A (2005) Modeling and analysis of PET studies with norepinephrine transporter ligands: the search for a reference region. Nucl Med Biol 32:531–542.

Lopez-Picon FR, Kirjavainen AK, Forsback S, Takkinen JS, Peters D, Haaparanta-Solin M, Solin O (2019) In vivo characterization of a novel norepinephrine transporter PET tracer [^{18}F]NS12137 in adult and immature Sprague-Dawley rats. Theranostics 9:11–19.

Marquis JM, Lettenberger SE, Kelm-Nelson CA (2020) Early-onset Parkinsonian behaviors in female Pink1-/- rats. Behav Brain Res 377:112175.

Miner LH, Schroeter S, Blakely RD, Sesack SR (2003) Ultrastructural localization of the norepinephrine transporter in superficial and deep layers of the rat prelimbic prefrontal cortex and its spatial relationship to probable dopamine terminals. J Comp Neurol 466:478–494.

Nahimi A, Kinnerup MB, Sommerauer M, Gjedde A, Borghammer P (2018a) Molecular imaging of the noradrenergic system in idiopathic Parkinson's disease. Int Rev Neurobiol 141:251–274.

Nahimi A, et al. (2018b) Noradrenergic deficits in Parkinson disease imaged with ^{11}C-MeNER. J Nucl Med 59:659–664.

National Research Council (2011) *Guide for the care and use of laboratory animals*, Ed 8. Washington (DC): National Academies Press.
Newman LA, Baraiolo J, Mokler DJ, Rabinowitz AG, Galler JR, McGaughy JA (2019) Prenatal protein malnutrition produces resistance to distraction similar to noradrenergic deafferentation of the prelimbic cortex in a sustained attention task. Front Neurosci 13:1–14.
Papp EA, Leergaard TB, Calabrese E, Johnson GA, Bjaalie JG (2014) Waxholm space atlas of the Sprague Dawley rat brain. Neuroimage 97: 374–386.
Paredes-Rodriguez E, Vegas-Suarez S, Morera-Herreras T, De Deurwaerdere P, Miguelez C (2020) The noradrenergic system in Parkinson's disease. Front Pharmacol 11:1–13.
Paxinos G, Watson C (1998) *The rat brain in stereotaxic coordinates*. San Diego: Academic Press.
Percie du Sert N, et al. (2020) The ARRIVE guidelines 2.0: Updated guidelines for reporting animal research. J Cereb Blood Flow Metab 40:1769–1777.
Pickrell AM, Youle RJ (2015) The roles of PINK1, parkin, and mitochondrial fidelity in Parkinson's disease. Neuron 85:257–273.
Poe GR, et al. (2020) Locus coeruleus: a new look at the blue spot. Nat Rev Neurosci 21:644–659.
Quinn PMJ, Moreira PI, Ambrósio AF, Alves CH (2020) PINK1/PARKIN signalling in neurodegeneration and neuroinflammation. Acta Neuropathol Commun 8:189.
Randver R (2018) Repetitive transcranial magnetic stimulation of the dorsolateral prefrontal cortex to alleviate depression and cognitive impairment associated with Parkinson's disease: a review and clinical implications. J Neurol Sci 393:88–99.
Richardson BD, Saha K, Krout D, Cabrera E, Felts B, Henry LK, Swant J, Zou M-F, Newman AH, Khoshbouei H (2016) Membrane potential shapes regulation of dopamine transporter trafficking at the plasma membrane. Nat Commun 7:10423.
Rudisch DM, Krasko MN, Burdick R, Broadfoot CK, Rogus-Pulia N, Ciucci MR (2023) Dysphagia in Parkinson disease: part I - pathophysiology and diagnostic practices. Curr Phys Med Rehabil Rep 11:176–187.
Sanders JD, Happe HK, Bylund DB, Murrin LC (2005) Development of the norepinephrine transporter in the rat CNS. Neuroscience 130:107–117.
Schou M, et al. (2009) Investigation of the metabolites of (S,S)-[C-11] MeNER in humans, monkeys and rats. Mol Imaging Biol 11:23–30.
Schroeter S, Apparsundaram S, Wiley RG, Miner LH, Sesack SR, Blakely RD (2000) Immunolocalization of the cocaine- and antidepressant-sensitive l-norepinephrine transporter. J Comp Neurol 420:211–232.
Seppi K, Ray Chaudhuri K, Coelho M, Fox SH, Katzenschlager R, Perez Lloret S, Weintraub D, Sampaio C (2019) Update on treatments for nonmotor symptoms of Parkinson's disease-an evidence-based medicine review. Mov Disord 34:180–198.
Sommerauer M, et al. (2018) Evaluation of the noradrenergic system in Parkinson's disease: an ^{11}C-MeNER PET and neuromelanin MRI study. Brain 141:496–504.
Tai YC, Chatziioannou A, Siegel S, Young J, Newport D, Goble RN, Nutt RE, Cherry SR (2001) Performance evaluation of the microPET P4: a PET system dedicated to animal imaging. Phys Med Biol 46:1845–1862.
Tejani-Butt SM (1992) [^{3}H]Nisoxetine: a radioligand for quantitation of norepinephrine uptake sites by autoradiography or by homogenate binding. J Pharmacol Exp Ther 260:427–436.
Torres GE, Gainetdinov RR, Caron MG (2003) Plasma membrane monoamine transporters: structure, regulation and function. Nat Rev Neurosci 4:13–25.
Vase KH, Peters D, Nielsen EO, Alstrup AKO, Bender D (2014) [C-11] NS8880, a promising PET radiotracer targeting the norepinephrine transporter. Nucl Med Biol 41:758–764.
Vertes RP (2004) Differential projections of the infralimbic and prelimbic cortex in the rat. Synapse 51:32–58.